JOURNAL OF GUIDANCE, CONTROL, AND DYNAMICS
Vol. 16, No. 2, March-April 1993

Fuel-Optimal Propulsive Reboost of Flexible Spacecraft

Larry Silverberg* and Jim Redmond†
North Carolina State University, Raleigh, North Carolina 27695

This paper presents for the first time an exact solution to the fuel-optimal propulsive reboost problem for flexible spacecraft. The spacecraft undergoes rigid-body motion and flexible-body motion, and reboost is achieved propulsively through the use of reaction control jets. The exact fuel-optimal solution to the associated minimization problem is found numerically based on an adaptive grid bisection search. The reboost of the floating harmonic oscillator reveals properties of the fuel-optimal solution. Nondimensional plots of minimum fuel vs maneuver time expose the nature of the solution classes depending on the maneuver time. Some very interesting properties are observed, among them the shifting of impulses to the smaller oscillator mass. Comparisons are made with near fuel-optimal solutions obtained by other investigators.

I. Introduction

THE prospect of placing large structures in space has stimulated interest in the problem of fuel-optimal control of flexible spacecraft. Of particular interest is fuel-optimal propulsive reboost of structures possessing significant structural flexibility.

In the early 1960s, in an extension of Krasovskii's geometric approach to optimal control theory,[1] Neustadt showed that fuel-optimal control of dynamic systems requires impulsive forces.[2] However, Neustadt was primarily concerned with broad classes of optimal control problems, particularly with those solved by gradient-based minimization procedures. Since fuel-optimal control does not fall under this category, Neustadt abandoned fuel-optimal control in favor of other minimization problems. Later on, Hajek re-examined fuel-optimal control but with the added constraint of bounded control inputs. Unlike the bang-bang form of time-optimal control,[3] he showed that bounded fuel-optimal control is bang-off-bang.[4]

Although fuel-optimal control was demonstrated successfully on a variety of low-order systems,[5-10] numerical difficulties plagued the solutions to fuel-optimal control of higher order systems (such as the reboost problem treated here). To circumvent these difficulties, various approaches have been adopted. One approach is to simply discard the fuel-optimal control formulation in favor of other more easily formulated techniques such as linear optimal control.[11] Other approaches render near fuel-optimal solutions by eliciting various properties associated with the fuel-optimal solution. For example, based on the premise that induced vibrations increase fuel consumption, reboost strategies that minimize flexural motion have been developed.[12] Also, the independent modal space control method[13] was employed to yield independent second-order modal fuel minimization problems. These problems were solved with relative ease, and the resulting optimal modal controls were then transformed to yield near optimal quantized actuator forces.[14] In other investigations, characteristics associated with the fuel-optimal solution of second-order systems were extended to more complicated systems. These investigations led to a feedback algorithm in which fuel-optimal pulses of reaction control jets act on the system at instances of peak local velocities.[15-18] This approach has been shown to be effective but once again is not based on an exact minimization. Indeed, the previously cited near fuel-optimal control solutions were developed because exact solutions were unavailable.

This paper provides the numerical foundation for the exact solution to the fuel-optimal control problem. The paper then focuses on the fuel-optimal propulsive reboost of flexible spacecraft. In particular, the fuel-optimal reboost of the floating harmonic oscillator problem is solved exactly. The solution exhibits some interesting properties. Among these properties, this paper reveals that the perceived properties on which the previously cited near fuel-optimal solutions were based are all violated to various degrees. Also, some new properties are exposed.

The fuel-optimal control problem is reviewed in Sec. II. Next, in Sec. III, an adaptive grid bisection search scheme is introduced for the minimization. The reboost problem is addressed in Sec. IV by introducing the floating harmonic oscillator as a tutorial spacecraft. The floating harmonic oscillator possesses one flexible-body mode and one rigid-body mode. A variety of examples is given. These include simple vibration suppression, rigid-body reboost, and general reboost. Finally, concluding remarks are given in Sec. V.

II. Fuel Optimal Control

Consider the linear time-invariant system

$$\dot{\boldsymbol{x}}(t) = A\boldsymbol{x}(t) + \sum_{j=1}^{m} \boldsymbol{b}_j u_j(t) \tag{1}$$

in which $\boldsymbol{x}(t)$ is the $n \times 1$ state vector. A is the $n \times n$ system matrix, $\boldsymbol{b}_j$ is the jth $n \times 1$ control participation vector, and $u_j(t)$ is the jth control input. The solution to Eq. (1) is

$$\boldsymbol{x}(t) = e^{At}\left(\boldsymbol{x}_0 + \sum_{j=1}^{m} \int_0^t e^{-As}\boldsymbol{b}_j u_j(s)\,\mathrm{d}s\right) \tag{2}$$

where $\boldsymbol{x}_0 = \boldsymbol{x}(0)$ is the initial state. The objective of the control is to transfer the system from the initial state $\boldsymbol{x}_0$ to a final state $\boldsymbol{x}_1 = \boldsymbol{x}(T_f)$ in maneuver time T_f. From Eq. (2), the reachable state is then defined as

$$\boldsymbol{y} = \sum_{j=1}^{m} \int_0^{T_f} e^{-At}\boldsymbol{b}_j u_j(t)\,\mathrm{d}t = e^{-AT_f}\boldsymbol{x}_1 - \boldsymbol{x}_0 \tag{3}$$

The fuel function associated with propulsive actuation is

$$\text{Fuel} = \sum_{j=1}^{m} \int_0^{T_f} |u_j(t)|\,\mathrm{d}t \tag{4}$$

Received Aug. 8, 1991; revision received April 1, 1992; accepted for publication June 2, 1992.

*Associate Professor, Mars Mission Research Center. Member AIAA.
†Graduate Research Assistant, Mars Mission Research Center. Student Member AIAA.

The fuel-optimal control transfers x_0 to x_1 in maneuver time T_f while minimizing the fuel.

The development of the fuel-optimal control solution is deeply rooted in set theory and beyond the scope of this paper. Thus, the details of this development have been omitted, leaving only the necessary results. (For those readers interested in the development, Refs. 2 and 10 provide a lucid introduction.) The control index functions are defined as

$$g_j(\eta, t) = \eta^T e^{-At} b_j \qquad j = 1, 2, \ldots, m \tag{5}$$

Here η is an $n \times 1$ vector contained in the hyperplane

$$H = \{\eta : \eta^T y = 1\} \tag{6}$$

where y is given in Eq. (3). The vector η is called the normal vector. Optimal control problems in general reduce to selecting a particular normal vector η from the hyperplane H that yields favorable characteristics associated with the control index functions $g_j(\eta, t)$. In the case of fuel-optimal control, we define the index extremum

$$\alpha^* = \min_{\eta \in H} \max_{1 \le j \le m} \sup_{0 \le t \le T_f} |g_j(\eta, t)| \tag{7}$$

The solution of Eq. (7) uniquely yields the optimal normal vector η^*. The fuel-optimal controls are of the form

$$u_j^*(t) = \frac{g_j^T c_j}{\alpha^*}, \qquad j = 1, 2, \ldots, m \tag{8}$$

in which g_j is an $N_j \times 1$ vector of impulses and c_j is an $N_j \times 1$ vector of impulse coefficients, given by

$$g_j = \{\operatorname{sgn}[g_j(\eta^*, \tau_{1j})]\delta(t - \tau_{1j}) \cdots \operatorname{sgn}[g_j(\eta^*, \tau_{N_j j})]\delta(t - t_{N_j j})\}^T \tag{9a}$$

$$c_j = [c_{1j} c_{2j} \cdots c_{N_j j}]^T \tag{9b}$$

The jth fuel-optimal control input $u_j^*(t)$ represents a series in time of N_j impulses. Here N_j $(j = 1, 2, \ldots, m)$ corresponds to the multiple solutions to Eq. (7) $\alpha^* = |g_j(\eta^*, \tau_{ij})|$ $(i = 1, 2, \ldots, N_j; j = 1, 2, \ldots, m)$. Note that N_j may be equal to zero for some j if $g_j(\eta^*, t)$ does not assume the value of α^* at any time during the maneuver. In this case, $u_j^*(t) = 0$. The impulse coefficients c_{ij} given in Eq. (9b) are nonnegative constants that satisfy

$$1 = \mathbf{1}^T c \tag{10}$$

where

$$c = [c_1^T c_2^T \cdots c_m^T]^T \tag{11a}$$

$$\mathbf{1} = [1 \;\; 1 \cdots 1]^T \tag{11b}$$

The impulse coefficients are chosen so that the resulting control accomplishes the stated objective, that is, such that the system is transferred from x_0 to x_1 in time T_f. In some cases, multiple solutions exist. Substituting Eq. (8) into Eq. (4), the minimal amount of fuel is

$$\text{Fuel}^* = \frac{1}{\alpha^*} \tag{12}$$

III. Numerical Solution by Adaptive Grid Bisection

The solution to Eq. (7) represents the primary difficulty associated with fuel-optimal control problems. Because in most cases α^* cannot be determined explicitly, the solution must be found numerically. Gradient methods are not applicable due to the nonlinearities and discontinuities present in Eq. (7). Fortunately, a relatively simple adaptive grid bisection search can be employed to obtain the index extremum α^*, the optimal normal vector η^*, the number of impulses N_j $(j = 1, 2, \ldots, m)$, the impulse times τ_{ij} $(i = 1, 2, \ldots, N_j; j = 1, 2, \ldots, m)$, and the impulse coefficients c_{ij} $(i = 1, 2, \ldots, N_j; j = 1, 2, \ldots, m)$.

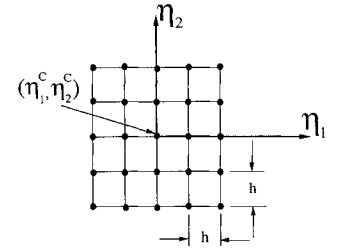

Fig. 1 Square grid generated in step 1 in which $n = 3$ and $L = 2$.

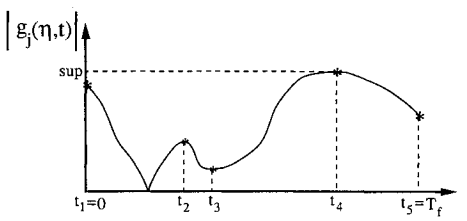

Fig. 2 Sample function for step 2 supremum computation.

The solution to Eq. (7) is found in the following seven steps:

1) Generate a square grid G of normal vectors $\eta_1, \eta_2, \ldots, \eta_p$ that form a subset of the hyperplane H.

2) Determine

$$\alpha_{ij} = \sup_{0 \le t \le T_f} |g_j(\eta_i, t)|$$

for each $\eta_i (i = 1, 2, \ldots, p)$ and for each $(j = 1, 2, \ldots, m)$. The suprema α_{ij} are computed to within the error margin ϵ_1.

3) Determine the grid-optimal normal vector η_i^* for which

$$\alpha = \min_{1 \le i \le p} \max_{1 \le j \le m} \alpha_{ij}$$

4) Select an updated grid G of normal vectors $\eta_1, \eta_2, \ldots, \eta_p$ centered about the grid-optimal normal vector η_i^* based on the following: a) If η_i^* is an interior grid point, decrease the grid spacing by 50% (bisection); and b) If η_i^* is a boundary grid point, increase the spacing by 50%.

5) Repeat steps 2–4 until the grid spacing is within the error margin ϵ_2. The converged grid-optimal normal vector represents the optimal normal vector η^*.

6) Determine the number of impulses N_j associated with $u_j^*(t)$ $(j = 1, 2, \ldots, m)$, the corresponding impulse times τ_{ij} $(i = 1, 2, \ldots, N_j; j = 1, 2, \ldots, m)$, and the sign functions $\operatorname{sgn}[g_j(\eta^*, \tau_{ij})]$ $(i = 1, 2, \ldots, N_j; j = 1, 2, \ldots, m)$.

7) Compute the impulse coefficients $c_{ij} (i = 1, 2, \ldots, N_j; j = 1, 2, \ldots, m)$.

In step 1, the hyperplane H is discretized into a square grid G. Recall that the hyperplane H is subject to the constraint $\eta^T y = 1$, so one of the n components of η is dependent, leaving $n - 1$ independent components. Without loss of generality, let the first $n - 1$ components be independent. The components $\eta_i (i = 1, 2, \ldots, n - 1)$ of η are now divided into $2L + 1$ components of points $\eta_i^{(r)} = \eta_i^C + rh (r = 0, \pm 1, \pm 2, \ldots, \pm L)$ centered at η_i^C with grid spacing h. The $n - 1$ dimensional square grid now contains $p = (2L + 1)^{n-1}$ grid points (see Fig. 1).

In step 2, the suprema

$$\alpha_{ij} = \sup_{0 \le t \le T_f} |g_j(\eta_i, t)|$$

$$(i = 1, 2, \ldots, p; j = 1, 2, \ldots, m)$$

are computed. Toward that end, candidate suprema (which include the suprema) are first computed. For each i and j, the candidate suprema include the two boundary points (in time) $|g_j(\eta_i, 0)|$ and $|g_j(\eta_i, T_f)|$ as well as local maxima. Note that $|g_j(\eta_i, t)|$ is normally continuous in time and infinitely differentiable except when $|g_j| = 0$ at which point $d|g_j|/dt$ changes its sign (see Fig. 2). As a consequence of these properties, the local maxima can be efficiently computed by means of bisections to approach the neighborhood of the local maxima followed by a Newton's method to converge to the local maxima to within the error margin ϵ_1. Note that these steps yield candidate suprema $\alpha_{ij}^{(k)}$ $(k = 1, 2, \ldots, N_{ij})$. Finally, the suprema themselves are obtained from

$$\alpha_{ij} = \max_{1 \le k \le N_{ij}} \alpha_{ij}^{(k)}$$

In step 3,

$$\alpha = \min_{1 \le i \le p} \max_{1 \le j \le m} \alpha_{ij}$$

is computed. This computation is trivial, not warranting explanation. The normal vector corresponding to α is referred to as the grid-optimal normal vector denoted by η_i^* where i is the grid index corresponding to α.

In step 4, the grid G is updated. The update is dependent on η_i^*. If η_i^* is an interior grid point, then the likelihood increases that the optimal normal vector η^* is contained within the boundaries of the existing grid in the neighborhood of the grid-optimal normal vector η_i^*. Thus a new grid is generated centered about η_i^* with the grid spacing decreased by 50% (see Fig. 3). However, if η_i^* is a boundary grid point, then the likelihood increases that η^* is not contained within the existing grid, in which case a new grid is generated centered about η_i^* with the grid spacing increased by 50% (see Fig. 4).

In step 5, steps 2-4 are repeated until the grid spacing is within the error margin ϵ_2. The converged grid-optimal normal vector is then taken as the optimal normal vector for the fuel-optimal control problem. The question arises here how to check whether the numerically converged grid-optimal normal vector is in fact the optimal normal vector. The answer to this question is provided by Eq. (12). Since the convergence to α^* is from above and fuel is inversely proportional to α^*, it follows that the fuel consumption converges from below. In the event that the converged α^* is not associated with the optimal normal vector, the associated converged fuel would be lower than the optimal fuel. In subsequent steps, this would lead to control inputs that cannot possibly transfer the system

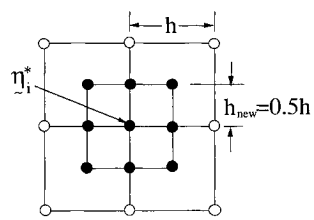

Fig. 3 Grid-optimal normal vector in the interior leads to the grid spacing decreased by 50% in step 4.

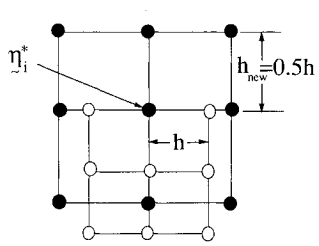

Fig. 4 Grid-optimal normal vector on the boundary leads to grid spacing increased by 50% in step 4.

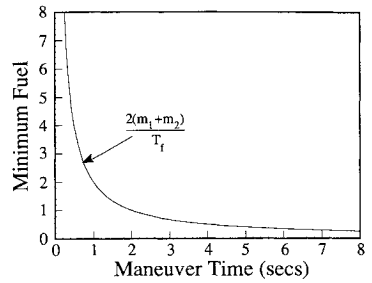

Fig. 5 Rigid-body reboost class: minimum fuel vs maneuver time.

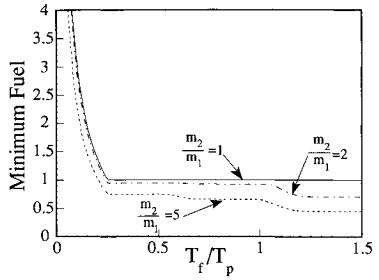

Fig. 6 Vibration suppression class: minimum fuel vs maneuver time.

from x_0 to x_1 in time T_f. On the other hand, if in subsequent steps the control inputs can transfer the system from x_0 to x_1 in time T_f, then the converged α is indeed α^* and is associated with the optimal normal vector.

In step 6, the optimal control inputs corresponding to η^* are computed. During the last iteration in step 5, the number of impulses N_j $(j = 1, 2, \ldots, m)$ associated with each $u_j^*(t)$, the impulse times τ_{ij} $(i = 1, 2, \ldots, N_j; j = 1, 2, \ldots, m)$, and the sign functions $\text{sgn}[g_j(\eta^*, \tau_{ij})]$ $(i = 1, 2, \ldots, N_j; j = 1, 2, \ldots, m)$ are recorded.

In step 7, the impulse coefficients c_{ij} $(i = 1, 2, \ldots, N_j; j = 1, 2, \ldots, m)$ are computed from a simultaneous set of linear algebraic equations. Substituting Eq. (8) into Eq. (3) and augmenting the result with Eq. (10), we obtain

$$\boldsymbol{P}\boldsymbol{c} = \boldsymbol{Q}, \qquad \boldsymbol{c} \ge \boldsymbol{0} \tag{13}$$

in which

$$\boldsymbol{P} = \left[\begin{array}{ccc} \frac{1}{\alpha^*}\int_0^{T_f}(e^{-At})\boldsymbol{b}_1\boldsymbol{g}_1^T\,dt & \cdots & \frac{1}{\alpha^*}\int_0^{T_f}(e^{-At})\boldsymbol{b}_m\boldsymbol{g}_m^T\,dt \\ \hline \multicolumn{3}{c}{\boldsymbol{1}^T} \end{array}\right] \tag{14a}$$

$$\boldsymbol{Q} = \left[\begin{array}{c} \boldsymbol{y} \\ \hline 1 \end{array}\right] \tag{14b}$$

Note that augmenting the reachable state equations with the condition of Eq. (10) as earlier is redundant if the true optimal normal vector has been determined. In this case, the converged index extremum α^* yields the optimal fuel via Eq. (12) only if Eq. (10) is satisfied. Nevertheless, Eq. (10) is included in the system because it gives an indication of the exactness of the optimal normal vector and the index extremum.

In general, rank (P) is less than or equal to n and the solution space is determined by row reduction. In instances when T_f is sufficiently small and the number of impulses is less than or equal to n, the system is uniquely determined. In other cases when T_f is sufficiently large, the number of im-

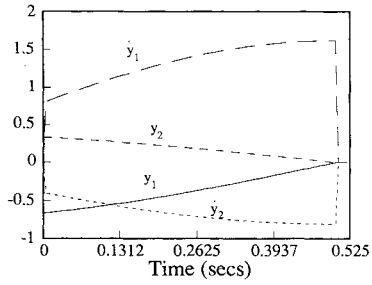

Fig. 7 Vibration suppression class, $m_2 = 2m_1$ case, $T_f = 0.5$ s: displacement and velocity of each mass vs time.

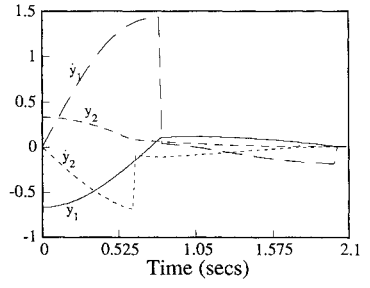

Fig. 8 Vibration suppression class, $m_2 = 2m_1$ case, $T_f = 2.0$ s: displacement and velocity of each mass vs time.

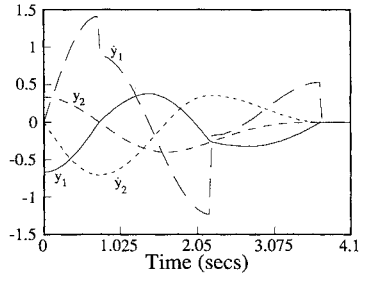

Fig. 9 Vibration suppression class, $m_2 = 2m_1$ case, $T_f = 4.0$ s: displacement and velocity of each mass vs time.

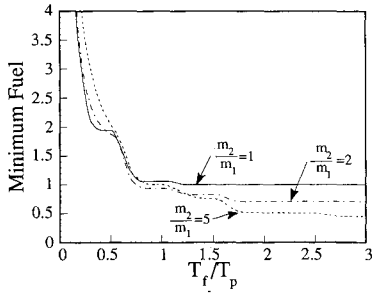

Fig. 10 General reboost class: minimum fuel vs maneuver time.

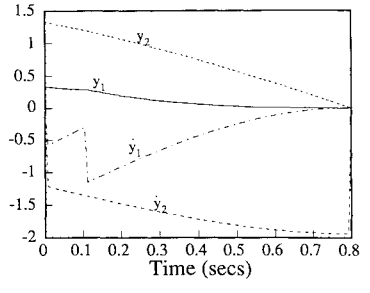

Fig. 11 General reboost class, $m_2 = 2m_1$ case, $T_f = 0.8$ s: displacement and velocity of each mass vs time.

pulse coefficients can be greater than n. In this case the system is underdetermined and multiple solutions exist. Also, note again that the nonexistence of an exact solution to Eq. (13) indicates that convergence to the optimal solution was not achieved in step 5.

IV. Floating Harmonic Oscillator

Of particular interest is the problem of fuel-optimal propulsive reboost of flexible spacecraft. The significant properties of the solution to this problem are revealed when we select the floating harmonic oscillator as an illustrative flexible spacecraft. This system consists of two masses, m_1 and m_2, undergoing displacements $y_1(t)$ and $y_2(t)$, respectively. The masses are linked by a linear spring of constant k and equipped with reaction control jets that produce control forces $u_1(t)$ and $u_2(t)$. The equations of motion are

$$m_1\ddot{y}_1(t) + k[y_1(t) - y_2(t)] = u_1(t) \tag{15a}$$

$$m_2\ddot{y}_2(t) + k[y_2(t) - y_1(t)] = u_2(t) \tag{15b}$$

Equation (15) is transformed into state-space form by defining the states

$$x_1(t) = \frac{m_1 y_1(t) + m_2 y_2(t)}{m_1 + m_2} \tag{16a}$$

$$x_2(t) = y_2(t) - y_1(t) \tag{16b}$$

$$x_3(t) = \dot{x}_1(t) \tag{16c}$$

$$x_4(t) = \dot{x}_2(t) \tag{16d}$$

where $x_1(t)$ represents the rigid-body displacement of the mass center and $x_2(t)$ represents the flexible-body displacement of the spring. The system is now recast in the form of Eq. (1), where

$$A = \begin{bmatrix} 0 & 0 & 1 & 0 \\ 0 & 0 & 0 & 1 \\ 0 & 0 & 0 & 0 \\ 0 & -\omega^2 & 0 & 0 \end{bmatrix} \tag{17a}$$

$$\boldsymbol{b}_1 = \begin{bmatrix} 0 \\ 0 \\ \dfrac{1}{m_1 + m_2} \\ \dfrac{-1}{m_1} \end{bmatrix} \tag{17b}$$

$$\boldsymbol{b}_2 = \begin{bmatrix} 0 \\ 0 \\ \dfrac{1}{m_1 + m_2} \\ \dfrac{1}{m_2} \end{bmatrix} \tag{17c}$$

in which

$$\omega = \sqrt{\frac{k(m_1 + m_2)}{m_1 m_2}}$$

Table 1 Control parameters: vibration suppression class, $m_2 = 2m_1$ case

		$u_1(t)$ impulses			$u_2(t)$ impulses		
T_f, s	α^*	τ_{1j}, s	sgn(g_1)	c_{1j}	τ_{2j}, s	sgn(g_2)	c_{2j}
0.5	0.621929	0.000000	+	0.164045	0.000000	−	0.164045
		0.500000	−	0.335955	0.500000	+	0.335955
2.0	1.080844	0.817892	−	0.498827	0.623410	+	0.436626
		2.000000	+	0.067895	—	—	—
4.0	1.414214	0.740480	−	0.250000	—	—	—
		2.221441	+	0.500000	—	—	—
		3.702402	−	0.250000	—	—	—

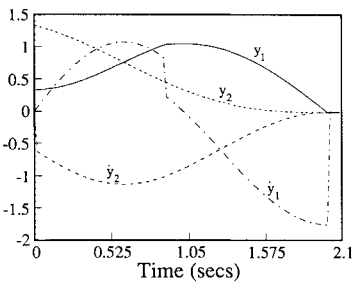

Fig. 12 General reboost class, $m_2 = 2m_1$ case, $T_f = 2.0$ s: displacement and velocity of each mass vs time.

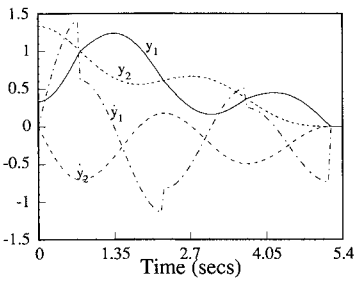

Fig. 13 General reboost class, $m_2 = 2m_1$ case, $T_f = 5.3$ s: displacement and velocity of each mass vs time.

denotes the natural frequency of the oscillation. The associated matrix exponential is

$$e^{At} = \begin{bmatrix} 1 & 0 & t & 0 \\ 0 & \cos \omega t & 0 & \dfrac{\sin \omega t}{\omega} \\ 0 & 0 & 1 & 0 \\ 0 & -\omega \sin \omega t & 0 & \cos \omega t \end{bmatrix} \tag{18}$$

Substituting Eqs. (17) and (18) into Eq. (5), we obtain

$$g_1 = \frac{-t}{m_1 + m_2}\eta_1 + \frac{\sin \omega t}{\omega m_1}\eta_2 + \frac{1}{m_1 + m_2}\eta_3 - \frac{\cos \omega t}{m_1}\eta_4 \tag{19a}$$

$$g_2 = \frac{-t}{m_1 + m_2}\eta_1 - \frac{\sin \omega t}{\omega m_2}\eta_2 + \frac{1}{m_1 + m_2}\eta_3 + \frac{\cos \omega t}{m_2}\eta_4 \tag{19b}$$

Next we examine the fuel-optimal solution associated with three classes of problems dependent on the sets of initial and final states. The three classes of problems are rigid-body reboost, vibration suppression, and general reboost. In all three classes of problems $x_0 = [x_{10}\ x_{20}\ 0\ 0]^T$, $x_1 = \mathbf{0}$, and we let $k = m_1 + m_2 = 1$. The reachable state is given from Eq. (3) as

$$y = [-x_{10}\ -x_{20}\ 0\ 0]^T \tag{20}$$

Substituting Eq. (20) into Eq. (6) yields the hyperplane constraint

$$-\eta_1 x_{10} - \eta_2 x_{20} = 1 \tag{21}$$

Rigid-Body Reboost Class

In the class of rigid-body reboost problems, each mass is displaced by one unit so $y_{10} = y_{20} = 1$, leaving the spring undeformed. From Eq. (16), $x_{10} = 1$ and $x_{20} = 0$. The exact solution to this fuel-optimal control problem is obtained in closed form. The optimal normal vector and the optimal control are given by

$$\eta^* = [-1\ 0\ -T_f/2\ 0]^T \tag{22}$$

$$u_j^*(t) = \frac{m_j}{T_f}[-\delta(t) + \delta(t - T_f)], \qquad (j = 1, 2) \tag{23}$$

As indicated by Eq. (23), the optimal control consists of an impulse on each mass at the initial and final times. The magnitudes of the impulses are proportional to mass. Because the inputs are proportional to mass, no vibration will be induced during the reboost. The minimum fuel is shown as a function of maneuver time in Fig. 5.

Vibration Suppression Class

In the class of vibration suppression problems, the two masses are displaced by the amounts $y_{10} = -m_2/(m_1 + m_2)$ and $y_{20} = m_1/(m_1 + m_2)$, leaving the system's mass center undisplaced. From Eq. (16), $x_{10} = 0$ and $x_{20} = 1$. The exact solution to this fuel-optimal control problem is obtained numerically. Consider the following three cases: 1) $m_2 = m_1$ ($\omega = \sqrt{4k}$), 2) $m_2 = 2m_1$($\omega = \sqrt{4.5k}$), and 3) $m_2 = 5m_1$($\omega = \sqrt{7.2k}$). The minimum fuel as a function of maneuver time is shown in Fig. 6 for all three cases. A single plateau is observed in the first case, and multiple plateaus are observed in the other two cases. The final plateau in each case extends to infinity. For the plateaus that extend to infinity, the pulse times do not change, but additional pulse times arise as the maneuver time is increased. The magnitudes of the associated pulses are not unique. With respect to each finite time plateau, the solution is the same over the associated range of maneuver times. Also note that as the maneuver time decreases below 50% of the natural period $T_p = 2\pi/\omega$, the minimum fuel required increases substantially in comparison with the minimum fuel for larger maneuver times.

The number and magnitude of the impulses associated with $u_j^*(t)(j = 1, 2)$ depend on the maneuver time as illustrated in Table 1. Table 1 shows three solutions corresponding to $m_2 = 2m_1$ ($T_p \approx 2.96$) and control times of 0.5, 2.0, and 4.0 s. As indicated for small maneuver times, impulses are applied on each mass at the initial and final times. For median maneuver times, fewer impulses are needed, and they are applied at intermediate times. As shown for $T_f = 2$ s, three impulses are applied each at different instances. Note that Eq. (10) is not exactly satisfied for this case. The sum of the impulse magnitudes is approximately 1.003. Thus, about 0.3% more fuel than the converged value is required to complete the maneuver. This numerical error is caused by the inexact determination of the index extremum α^* using adaptive grid bisection. In general, the degree to which Eq. (10) is satisfied signifies the degree of optimality of the control scheme. For larger maneu-

Table 2 Convergence example: vibration suppression class, $m_2 = 2m_1$ case $T_f = 2.0$ s

Iteration	η_1	η_3	η_4	Step size	Min max sup $\lvert g_j(\eta, t)\rvert$
1	0.000000000	0.000000000	0.000000000	1.0000000000	1.4142135623731
2	0.500000000	0.500000000	0.000000000	0.5000000000	1.3041415131743
3	0.500000000	0.750000000	0.000000000	0.2500000000	1.1265267495443
4	0.500000000	0.750000000	0.000000000	0.1250000000	1.1265267495443
5	0.500000000	0.687500000	0.062500000	0.0625000000	1.1009325628443
10	0.410156250	0.656250000	−0.013671875	0.0019531250	1.0811093227742
20	0.408424377	0.655029297	−0.013526916	0.0000171661	1.0808406732402
35	0.408419866	0.655029163	−0.013533452	0.0000000141	1.0808403397486
45	0.408419879	0.655029163	−0.013533430	0.0000000001	1.0808403395831

Table 3 Control parameters: general reboost class, $m_2 = 2m_1$ case

		$u_1(t)$ impulses			$u_2(t)$ impulses		
T_f, s	α^*	τ_{1j}, s	sgn(g_1)	c_{1j}	τ_{2j}, s	sgn(g_2)	c_{2j}
0.8	0.387717	0.000000	−	0.077500	0.000000	−	0.310394
		0.110495	−	0.112258	0.800000	+	0.500151
2.0	0.849176	0.891020	−	0.164744	0.000000	−	0.337958
		2.000000	+	0.497984	—	—	—
5.3	1.414214	0.740480	−	0.377465	—	—	—
		2.221441	+	0.150000	—	—	—
		3.702402	−	0.122535	—	—	—
		5.183363	+	0.350000	—	—	—

ver times the impulses tend to be applied only on the smaller mass. As shown for $T_f = 4$ s, three impulses are applied at intermediate times. An investigation of the solution for various maneuver times reveals that for large maneuver times the optimal control forces are applied only on the smaller mass when its velocity is at a peak. The time responses associated with the three solutions are shown in Figs. 7–9. Also, the grid-optimal normal vectors associated with the numerical optimization for $T_f = 2.0$ s are given in Table 2.

General Reboost Class

In this class of problems, both rigid-body and flexible-body initial displacements are present. Let $x_{10} = 1$ and $x_{20} = 1$ and consider the following three cases: 1) $m_2 = m_1$, 2) $m_2 = 2m_1$, and 3) $m_2 = 5m_1$. The minimum fuel as a function of maneuver time is shown in Fig. 10 for all three cases. Note that, as the maneuver time decreases, the minimum fuel associated with general reboost becomes the minimum fuel associated with rigid-body reboost as shown in Fig. 5. Furthermore, as the maneuver time increases, the minimum fuel associated with general reboost becomes the minimum fuel associated with vibration suppression as shown in Fig. 6. Also, note the existence of plateaus in each case. Once again, these plateaus represent either identical or multiple solutions as interpreted in the previous class of problems. As shown, when the maneuver time decreases below the natural period T_p, the minimum fuel required increases substantially. The number and magnitude of the impulses associated with $u_j^*(t)(j = 1, 2)$ depend on the maneuver time as illustrated in Table 3 for $m_2 = 2m_1$. Table 3 shows three solutions depending on the maneuver time. As indicated, the impulses shift to the first mass as the maneuver time increases. Figures 11–13 show the time responses for the three cases.

V. Conclusions

This paper presented a numerical technique for exactly solving the fuel-optimal control problem of high-order systems. Furthermore, the exact solution to the fuel optimal reboost of the floating harmonic oscillator was carried out and subsequent properties were revealed.

Many of these properties were previously observed in the near fuel-optimal solutions formulated by other investigators whereas others were not. The guiding principles of the independent control of modes and the prevention of induced vibration were both observed in the rigid-body reboost case. The guiding principle of impulse damping at peak velocities was observed in all of the pertinent cases for large maneuver times. However, these guiding principles of the near fuel-optimal solutions conflict with the exact solution in other cases. In the case of vibration suppression, the fuel-optimal solutions utilized the rigid-body motion that violates the principle of the independent control of modes. Additional properties revealed by the exact solution include the tendency for the actuation to be concentrated at the smaller mass, the existence of multiple solutions in the case of vibration suppression for large maneuver times, and the repetition of solutions over ranges of maneuver times.

Acknowledgments

This research was supported by NASA Grant NAGW-1331 to the Mars Mission Research Center and NASA Grant NAG1-977 monitored by Raymond Montgomery.

References

[1]Krasovskii, N. N., "On the Theory of Optimum Control," *Journal of Applied Mathematics and Mechanics,* Vol. 23, No. 4, 1959, pp. 899–919.

[2]Neustadt, L. W., "Minimum Effort Control Systems," *SIAM Journal on Control,* Vol. 1, No. 1, 1962, pp. 16–31.

[3]Neustadt, L. W., "Synthesizing Time Optimal Control Systems," *Journal of Mathematical Analysis and Applications,* Vol. 1, 1960, pp. 484–493.

[4]Hajek, O., "L_1-Optimization in Linear Systems with Bounded Controls," *Journal of Optimization Theory and Applications,* Vol. 29, No. 3, 1979, pp. 409–436.

[5]Athanassiades, M., "Optimal Control for Linear Time-Invariant Plants with Time, Fuel, and Energy Constraints," *Transactions of the American Institute of Electrical Engineers,* Vol. 891, Pt. II, Applications and Industry, 1962, pp. 321–325.

[6]Athans, M., "Minimum-Fuel Feedback Control Systems: Second-Order Case," *IEEE Transactions on Applications and Industry,* No. 65, March 1963, pp. 8–17.

[7]Athans, M., "Fuel-Optimal Control of a Double Integral Plant," *IEEE Transactions on Applications and Industry,* Vol. 83, No. 73, July 1964, pp. 240–246.

[8]Meditch, J. S., "On Minimum-Fuel Satellite Attitude Controls," *IEEE Transactions on Applications and Industry,* Vol. 83, March 1964, pp. 120–128.

[9]Athans, M., "Minimum-Fuel Control of Second-Order Systems with Real Poles," *IEEE Transactions on Applications and Industry,* Vol. 83, No. 72, May 1964, pp. 148–153.

[10]Redmond, J., and Silverberg, L., "Fuel Consumption in Optimal Control," *Journal of Guidance, Control, and Dynamics*, Vol. 15, No. 2, 1992, pp. 424–430.

[11]Athans, M., and Falb, P. L., *Optimal Control—An Introduction to the Theory and Its Applications,* McGraw-Hill, New York, 1966.

[12]Foster, L. A., and Mapar, J., "Control Structure Interaction for Space Station Freedom Early Assembly Flights," AAS/AIAA Spaceflight Mechanics Meeting, AAS Paper 91-146, Houston, TX, Feb. 11–13, 1991.

[13]Meirovitch, L., and Baruh, H., "Control of Self-Adjoint Distributed Parameter Systems," *Journal of Guidance, Control, and Dynamics,* Vol. 5, No. 1, 1982, pp. 60–66.

[14]Shenhar, J., and Meirovitch, L., "Minimum Fuel Control of Higher Order Systems," *Journal of Optimization Theory and Applications,* Vol. 48, No. 3, 1986, pp. 469–491.

[15]Silverberg, L., "Light Impulsive Damping of Spacecraft Exhibiting Normal Mode Behavior," *Journal of Guidance, Control, and Dynamics,* Vol. 15, No. 1, 1992, pp. 114–120.

[16]Foster, L. A., III, and Silverberg, L., "On-Off Decentralized Control of Flexible Structures," *Journal of Dynamic Systems, Measurement and Control,* Vol. 113, March 1991, pp. 41–47.

[17]Meyer, J. L., "Experimental Verification of Impulse Damping Control," M.S. Thesis, North Carolina State Univ., Raleigh, NC, May 1990.

[18]Redmond, J., Meyer, J. L., and Silverberg, L., "Fuel Optimal Control of an Experimental Multi-Mode System," *Proceedings from the Eighth VPI&SU Symposium on Dynamics and Control of Large Structures* (Blacksburg, VA), May 6–8, 1991.